Experimental investigation of processing disturbances in laser surface patterning

Garcia Giron, Antonio; Romano, Jean-Michel; Batal, Afif; Michalek, Aleksandra; Penchev, Pavel; Dimov, Stefan

Document Version
Peer reviewed version

Experimental investigation of processing disturbances in laser surface patterning

A. Garcia-Giron[1],*, J. M. Romano[1], A. Batal[1], A. Michałek[1], P. Penchev[1] and S.S. Dimov[1]

[1]Department of Mechanical Engineering, School of Engineering, University of Birmingham, Edgbaston, Birmingham, B15 2TT, UK

*Corresponding author: Tel: +44 (0) 7843 859099; E-mail: antoniogarciagiron@gmail.com

ABSTRACT

Laser surface patterning has attracted a significant interest from industry and research due to its promising applications in surface functionalisation. However, there are specific issues and limitations associated with the beam delivery, especially when processing 3-D surfaces and/or setting up routines for executing complex multi-axis processing strategies. In particular, there are common processing disturbances that affect the resulting surface topographies and profiles and their respective functional responses, i.e. geometrical distortions of resulting surface patterns, focal offset distance (FOD) and variations of beam incident angle (BIA). A method to investigate the effects of these factors in laser patterning 3-D surfaces is presented in this research, especially how their effects can be analysed independently by conducting empirical studies on planar surfaces. A pilot implementation of the proposed methodology is reported for producing channel-like patterns on stainless steel plates with a super-hydrophobic functional response. The results are discussed in detail to show how the effects of processing disturbances on topographies, profiles and areal parameters together with the respective functional responses of patterned planar surfaces can be analysed and then used to set constraints in pre-processing 3-D surfaces for follow up laser patterning.

1. Introduction

There is constant drive for improving the performance of existing products and also for integration of more functions in new products due to competitive advantages that such advances offer to companies. Therefore, technologies that can be deployed for improving the performance of products have attracted a significant interest from industry and research. An important group of such technologies have been applied successfully to functionalise surfaces and thus to improve and/or integrate novel and attractive properties into existing and new products, e.g. to incorporate surfaces exhibiting anti-icing [1], anti-bacterial [2], cell growth enhancement [3], hydrophobic [4] and friction reduction [5] properties. One of the common objectives in such applications is to control the wetting response of functionalised surfaces [6] as it is often related to other properties [7,8], i.e. corrosion resistance [9], ice repellence [10] or self-cleaning [11].

One of the technologies that have attracted a significant industrial and research interest, recently, is the laser patterning process, especially as a tool for selective functionalisation of surfaces. And, this is not surprising taking into account its flexibility and capabilities to achieve high accuracy, repeatability, reproducibility and efficiency [12,13] in processing different materials. Furthermore, the laser processing does not require the use of any chemical substances and also as a non-contact technology there is only a negligible material waste. Therefore, it is considered an environmentally friendly process [14]. Moreover, laser surface functionalization can be applied on a wide range of materials, from metals [15,16] to polymers [17], and thus can be deployed in different industrial sectors, e.g. in aeronautics, automotive or medical applications.

Laser-based surface functionalization has been widely studied by many research groups but most of them have been focused on processing planar surfaces. At the same time, it is recognised that laser patterning of 3-D surfaces is a challenging task that requires complex multi-axis beam delivery systems and therefore has been investigated by a number of researchers, recently. In particular, Diaci et. al. developed a method for engraving curved and tilted surfaces that employed a sensor for measuring the shape of workpieces before the laser processing [18]. Overmeyer et. al. reported the fabrication of sensors on tilted and freeform surfaces and showed interdependences between the beam incident angle (BIA) and respective fluence and reflectance variations that affected the laser-material interactions [19]. Cuccolini

et. al. created a method employing a 5 axis CAM procedure for laser milling of 3-D surfaces, especially by partitioning surfaces into overlapping triangular areas to generate beam paths and control/synchronise the movements of the mechanical axes and beam deflectors [20]. Jiang et. al. proposed another method that again generated the scanning paths by partitioning free form surfaces and then the necessary programmes for positioning scan heads and for controlling a five axes gantry machine tool while processing each working area [21]. In another research, Wang et. al. investigated the effects of surface curvature on beam spot shape and energy distribution at the focal point and then used the results to develop a method for partitioning surfaces and thus to laser process them with required accuracy and quality [22].

The focus of all these investigations was predominantly on developing methods for partitioning 3-D surfaces into fields and then generating the necessary scanning paths for processing each of them following a pre-determined sequence of scan head positions. In particular, these methods generate the necessary beam paths and strategies for laser processing 3-D surfaces but without investigating systematically the factors or processing disturbances that can affect the laser patterning process and ultimately the functional response of the resulting surface topographies. For example, Fig. 1 a-b depicts a laser processing setup where a 3-D surface is approximated/tessellated into planar fields and each of them is laser processed sequentially. In particular, each field is approximated with a discrete planar field (the red line segments of the curved surface) with different relative angles between their normals and the laser beam (α_0, α_1, α_2...). Thus, if this laser processing approach is adopted for patterning 3-D surfaces three factors can affect the resulting topographies and their respective functional response, i.e. focal offset distance (FOD), BIA and spatial differences between the nominal and produced patterns on 3-D surfaces, also referred as geometrical distortions in this research. These factors can be considered as processing disturbances, too, and their effects should be investigated independently, e.g. by patterning planar surfaces/fields that approximate 3-D surfaces as illustrated in Fig. 1c.

The processed area of any conventional beam deliver system that integrates a F-theta scan lens is determined in size by its field of view while the pattern quality is affected by its theoretical depth of focus (DOF), defined as two times the Rayleigh range [23]:

$$DOF = \frac{2\pi(\omega_0)^2}{(M^2)\lambda} \tag{1}$$

where: ω_0 is the radius of the beam spot at the focal plane, M^2 - the beam quality factor and λ - the laser wavelength. Thus, as depicted in Fig. 1, when an area on a 3-D surface approximated as a tessellated field is processed some points on the workpiece will be in focus, e.g. Point A, while others will be outside of the respective lens's DOF, e.g. Point B (see Fig.1). Sola et. al. demonstrated that laser ablation yields are very dependent on FOD [24,25]. Thus, when a beam delivery system that integrates a F-theta lens is used to process a 3-D surface, homogeneity of the resulting patterns is affected [26].

The other disturbance commonly present when processing 3-D surfaces are deviations of BIA (α) from normal. BIA affects the resulting surface patterns and thus the final topography and potentially its functional response due to three reasons mainly, i.e.: i) alterations in reflectance and fluence [19], ii) the fluid mechanics of the molten material when ns and ms laser sources are utilised, and iii) the evacuation of ablated material from the produced patterns [27].

Finally, the other factor that affects the resulting patterns on 3-D surfaces and potentially again their functional response are some geometrical distortions. Such distortions are caused again by deviations of BIA from normal due to the surface curvature, but it is worth investigating their effects separately. For example, as shown in Fig. 1c, the nominal design of a channel-like pattern requires the distances between the channels to be equal to Δl however due to the deviation of BIA, α, from normal the distance will be $\Delta l'$, in particular:

$$\Delta l' = \frac{\Delta l}{cos\alpha} \tag{2}$$

Thus, the patterns produced with BIA different from normal will be always distorted compared with their nominal design.

These three processing disturbances can affect not only the patterns created on 3-D surfaces, but also on any surface when it is not correctly positioned in respect to the focal plane (see Fig. 1c), or when the beam delivery system is not properly calibrated. In this research, a method to investigate the effects of these three factors in laser patterning 3-D surfaces is presented, especially how their effects can be analysed independently by conducting empirical studies on planar surfaces. A pilot implementation is reported, especially by applying the proposed methodology for producing channel-like patterns on stainless steel plates with a super-hydrophobic functional response. The results are discussed in detail to illustrate how the effects of processing disturbances on topographies, profiles and areal parameters together with the

respective functional responses of patterned planar surfaces can be analysed and then used to set constraints in pre-processing 3-D surfaces for follow up laser patterning.
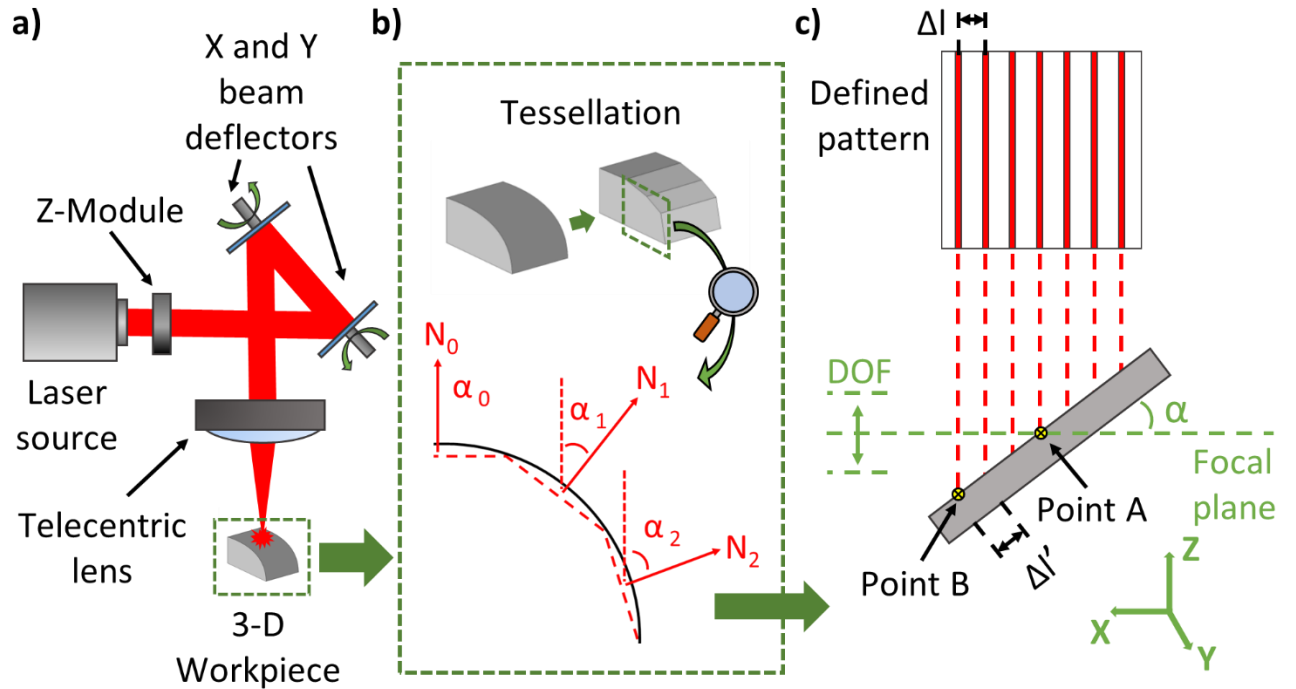
Fig. 1. The laser processing setup (a) employed to produce channel-like patterns on: b) 3-D and c) planar surfaces.

2. Methods and Experiments

2.1. Methodology

A methodology is proposed to study the effects of processing disturbances in laser patterning 3-D surfaces. Fig. 1b shows a general case of a free-form surface (the black curve) which has to be laser patterned. All three factors affecting the laser patterning process are present in this case, i.e. pattern distortions and FOD and BIA variations. Therefore, a common solution to limit their effects on resulting topographies and hence on their respective functionalities, too, is to pre-process such 3-D surfaces by partitioning/tessellating them into planar fields. For example, the 3-D surfaces can be represented by triangular and square fields, for follow up laser patterning as depicted in Fig. 1b, i.e. where the planar fields are represented by line

segments of the curve [20,21]. However, the processing disturbances will be still present when patterning 3-D surfaces partitioned into planar fields (see Fig. 1c) together with their effects on topography and functionality. Therefore, the effects of each disturbance should be investigated independently while patterning planar surfaces and so to inform/guide partitioning/tessellation processes by setting constraints. In particular, three different sets of samples on planar surfaces can be produced to investigate their effects independently. Especially, the samples in each set can be patterned by varying the values of only one factor at a time as follows:

- *Pattern distortion*: For example, the distance between the channels will vary when patterning a 3-D surface as shown in Fig. 1c due to variations of BIA. To investigate this factor independently from the BIA variation a set of samples should be patterned in focus with a beam normal to the surface while the distance between channels should be varied gradually, e.g. as in the pilot implementation of the proposed methodology from 100 to 350 µm with an increment of 50 µm.

- *FOD*: When patterning a field on a 3-D surface, the FOD will depend on the set focal plane as shown with the green line in the general case depicted in Fig. 1c while the other two factors will be present, too. Therefore, a set of samples should be patterned with a beam normal to the surface without any pattern distortion. For example, in the pilot implementation the channel distance was maintained at 100 µm while only FOD was varied along the Z axis from 0 (patterning in focus) with an increment of 250 µm, both above and below the focal plane. The FOD convention sign in this research was positive when the focal plane was above the sample and negative when it was below.

- *BIA*: Again, to investigate independently the BIA effects in patterning 3-D surfaces from other two factors, a set of samples should be patterned in focus without any pattern distortion, e.g. constant channel distance, while varying only BIA.

Then, the resulting topographies on the samples in each of the three sets should be analysed to determine quantitatively if there are any deviations due to the considered three factors. For example, Fig. 2a-c depicts representative profiles on the three sets of samples produced in the pilot implementation of the proposed methodology. By analysing them it is possible to determine the deviations caused by each factor (the continuous coloured profiles in the figure) in comparison to the reference pattern (the black dashed profiles), i.e. the profiles of a sample produced at focus, with normal BIA and without pattern distortion, i.e. with the nominal channels' distance, respectively.
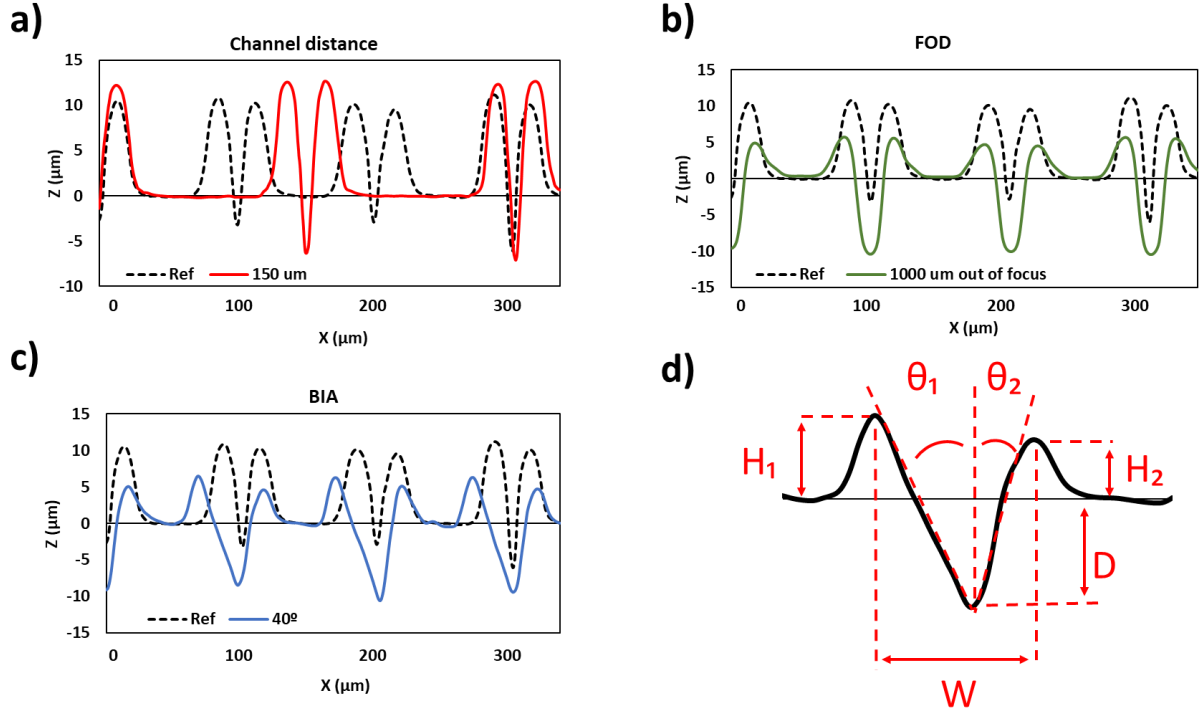
Fig. 2. Representative examples of profiles for the three sets of samples produced with: a) varying channel distance, b) FOD, c) BIA and d) the different surface parameters measured on profiles of the samples produced with BIA deviations. The black dashed lines represent the reference sample produced at focus with 100 μm distance between lines and BIAS of 0°while the coloured solid lines represent the patterns' profiles.

In particular, the surface profiles of the samples can be analysed quantitatively by calculating the deviations (Dev [%]) of surface profiles in respect to the reference one, using the following equation:

$$Dev\ (\%) = \frac{|Ref - Measured|}{Ref} 100 \tag{3}$$

where: Ref is the value of the considered surface profile parameters, e.g. D, W, H_1, H_2, θ_1 or θ_2 in Fig. 2d, obtained on the reference sample, and $Measured$ are the respective values obtained on profiles produced when the processing disturbances were present, i.e. the increasing FOD and the BIA deviation from normal.

Altogether, the effects of the considered three factors on surface functionality should be used to set limits on any considered profile variations in order to obtain acceptable results when processing 3-D surfaces. In particular, the results from the investigated dependences between

the surface functional response, e.g. its wettability, and the considered three processing disturbances can be used to set limits on channel distortions, FOD and the BIA deviations when patterning 3-D surfaces (see Fig. 1). Then, indirectly through these limits, it will be possible to set constraints in pre-processing 3-D surfaces, i.e. to drive their partitioning/tessellation into planar fields, for follow up laser patterning. For example, the maximum offset of the fields representing the 3-D surface, i.e. the distance between the line segments and the surface in Fig. 1, can be set at a given value in order to retain the desired functional response. In addition, the results can be entered in proprietary software as Smartpatch [28] and CALM [29] to optimise the partitioning process, e.g. to minimise the laser patterning time.

2.2. Experiments

A pilot implementation of the proposed methodology required three set of samples to be produced as described in Section 2.1. The patterns selected for this empirical study are channel-like structures that are commonly used and also investigated by many researchers for fabricating surfaces with a hydrophobic functional response [30–33].

The three set of samples were patterned using a SPI redEnergy G4 50W HS-S MOPA-based Yb-doped fibre nanosecond (ns) source with a wavelength of 1064 nm and circular polarisation, integrated into a laser micro-machining (LMM) platform. The laser source had M^2 better than 1.2 and a maximum repetition rate of 1MHz, while the pulse duration could be modulated from 15 to 220 ns. The beam delivery system of the LMM platform integrates a 3-D scan head, i.e. a Z-module and X and Y beam deflectors (RhoThor RTA), and a 100 mm telecentric focusing lens (See Fig. 1). A spot size of 35 µm was obtained at focus on this system, while the maximum achievable scanning speed was 2.5 m/s. Furthermore, the 3D scan head through the use of the Z-module allowed high dynamics movements of the focal plane in a range up to 7.7 mm along the lens' axis and thus to enable laser processing within a 35 x 35 x 7.7 mm volume.

In addition, the LMM platform integrates a stack of mechanical stages that allows the sample positioning in X, Y and Z together with rotary movements around X and Z axis, with positioning resolutions of 0.25 µm and 45 µrad, respectively. In the pilot implementation of the proposed methodology the Z stage was used to investigate the FOD effects, i.e. to reposition the focal plane along the Z axis. At the same time, the X rotary stage was used to vary BIA with an increment of 5º. Especially, after setting up the samples at a given BIA, the Z-module

of the 3-D scan head was used to reposition the focal plane when processing each channel [23]. At the same time, the nominal distance between channels (Δl) was varied to keep the actual distance ($\Delta l'$) on the produced samples the same, i.e. 100 µm (see Fig. 1).

Also, the LMM platform was equipped with a confocal displacement sensor, i.e. a CCS Prima sensor, for positioning the processed surfaces, especially for setting up very accurately the origins of samples' coordinate systems in regard to the focal plane. However, it was necessary to limit the maximum BIA investigated in this research to 40º due to limitations of the used setting up procedure, especially the reflectivity of the stainless steel plates impeded the correct performance of the confocal sensor when the tilting angle was bigger than 40º.

All samples in the three sets were produced on ferritic stainless steel X6Cr17 plates with 0.7 mm thickness and a diameter of 36 mm. The same laser processing parameters were used to pattern all samples and they were selected based on previous results [28]. Especially, channel-like patterns were produced by consecutive parallel scans of the laser beam with a speed of 150 mm/s while the distance between scanned lines was 100 µm. Pulse duration was set at 220 ns to produce deeper channels and higher bulges, i.e. the deposited molten material on the sides of the channels. Pulse repetition rate and energy were set at 70 kHz and 172.1 µJ, respectively. Each sample was produced 3 times, and 3 different measurements in different areas of the patterned surfaces were taken, and thus 9 measurements in total were obtained from each sample. Then, the average values with their standard deviations were calculated based on these 9 measurements.

The produced patterns were analysed with SEM micrographs created using a JEOL JCM-600 Benchtop Scanning Electron Microscope. An Alicona G5 focus variation microscope was utilized to inspect the patterned areas. In particular, the effects of investigated three factors on areal surface parameters and 3D topographies of the patterned surfaces were analysed using a x20 magnification lens, with a vertical resolution of 50 nm. Surface topographies of the samples were captured and the profiles of the patterns, cross-sections perpendicular to the channels, were measured using the Profile Form Measurement tool integrated in the Alicona software, which calculates the average values of considered profile parameters. Especially, the specific measurements taken on the samples produced in the pilot implementation of the methodology (see Fig. 2) were the depth (D) and width (W) of the channels, and the height of the bulges (H). Regarding the set of samples produced with different channel distances, only the areal surface parameters were studied, as the profile differences were marginal. For the set

of samples produced with the BIA deviations, the channels' profiles were not symmetric, and therefore the height of the bulges on both sides was analysed separately, i.e. as H_1 and H_2 in Fig. 2d. Furthermore, the tapering angles of the channels' walls were different, in particular bigger on one side (θ_1) and smaller on the other (θ_2). It should be noted that the bigger H_1 and θ_1 were for the wall side incident to the beam.

Furthermore, the areal surface parameters were obtained for each sample, in particular, the arithmetic mean height of the surface (Sa) and the true to projected area ratio (Ar) were found relevant, and were analysed further in this research. Ar was selected because this areal parameter represents the relation between the true area of a surface and its projected area and provides information about the aspect ratio of the patterns that affects the wettability of surfaces [6]. Pearson correlation analysis was conducted to identify potential correlations between the three disturbances and areal parameters and functionality of patterned surfaces.

All together, the impact of investigated processing disturbances on functional responses of patterned surfaces were studied by measuring the static contact angles (CA) with an optical tensiometer, i.e. Attension Biolin Scientific Theta T2000-Basic+, with 6 µl Milli-Q water droplets. It is worth noting that samples were only cleaned with compressed air after the laser patterning to remove debris. No chemicals were used to clean the surfaces to avoid surface contamination and any other side effects. Samples were kept in plastic boxes in ambient conditions, and the contact angles were measured after one month.

3. Results and discussion

The results from the pilot implementation of the proposed methodology obtained from the three set of samples produced as described in Section 2.2 are reported and discussed in this section. Especially, the effects of channel distance, FOD and BIA on surface topography, profiles, surface parameters and functional response together with their potential use in partitioning 3-D surfaces are reported and discussed.

3.1. Effects on surface topography

The effects of the investigated three factors, i.e. channel distance, FOD and BIA, on resulting surface topographies are depicted in Fig. 2. Especially, the resulting topographies on the

samples produced by varying channel distance, FOD and BIA from 100 µm, 0 mm and 0 degrees to 150 µm, 1 mm and 40 degrees, respectively, are provided there. The SEM micrographs of the same samples shown in Fig. 2 are given for comparison in Fig. 3. Fig. 3a-b depict the reference pattern that corresponds to the black dashed profile in Fig. 2.
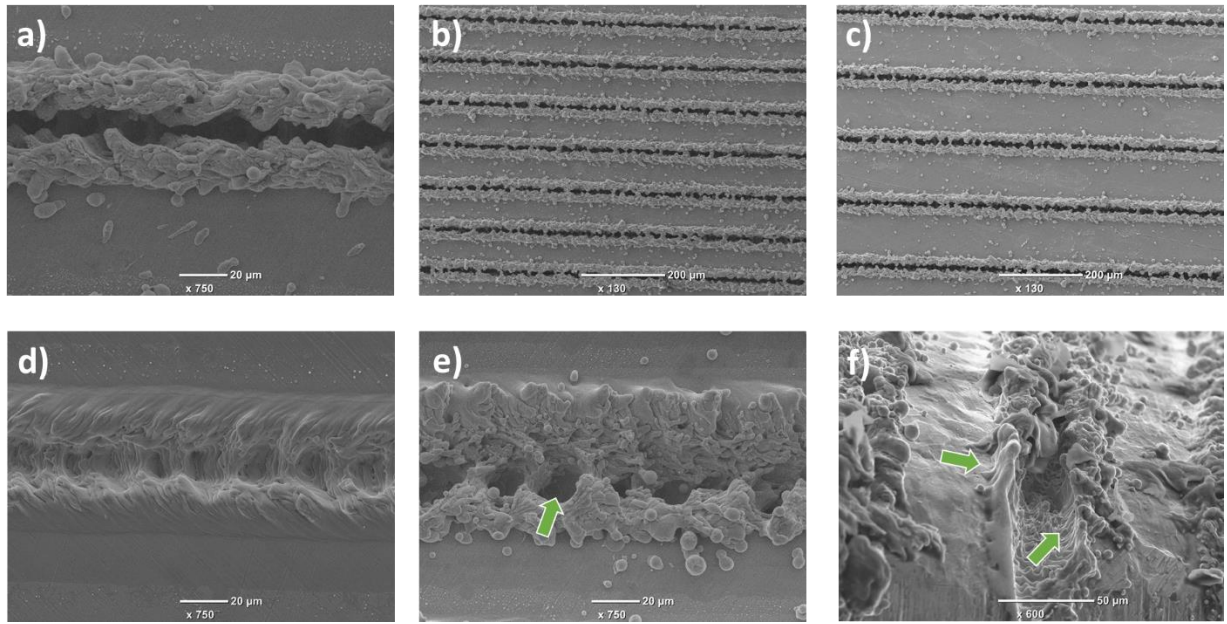

Fig. 3. SEM micrographs of channels on a reference sample produced with 100 µm distance between them and without FOD and BIA deviations in a) and b) with x750 and x130 magnifications, respectively. SEM micrographs of channels on samples produced with: c) an increased distance between them to 150 µm, d) FOD of 1 mm, and e-f) BIA of 40°.

As expected, due to relatively high thermal load when a nanosecond laser is used, the channels are surrounded by bulges, i.e. depositions of molten material along the beam path. As a result of the quick solidification the bulges are relatively rough and porous and this can explain the changes of wetting properties, especially the transition to hydrophobicity of patterned surfaces [15, 28].

The analysis of micrographs in Fig. 3b-c suggest that the change of the channel distance from 100 to 150 µm did not affect the resulting topography and therefore are not discussed further. At the same time, FOD of 1 mm led to a clear increase of channels' width and depth, while the resulting bulges were less pronounced compared to the reference pattern (see Fig. 2b and Fig. 3d) and also the porosity was greatly reduced. As a result of the other processing disturbance,

i.e. the BIA increase to 40º from normal, the channel profiles were not symmetrical anymore (see Fig. 2c and Fig. 3e-f). In particular, the deposition of ablated and melted material led to different bulges' height and tapering angles along the channels, especially a higher deposition and bigger tapering angles were observed on the beam incident wall side. This can be explained with the competing phenomena when laser processing is performed with a beam not normal to the surface, especially due to alterations in reflectance and fluence [19], the fluid mechanics of the molten material and also one sided evacuation of ablated material from the channels [27]. In addition, it is worth noting that there were some deep craters and even some small undercuts formed on the channels' side opposite to the beam incident one where the melted material was evacuated (see green arrows in Fig. 3e-f).

3.2. Effects on surface profiles

The laser patterns produced in the presence of FOD and BIA deviations were compared with the reference one, i.e. processed at focus with a beam normal to the surface.

3.2.1. FOD effects

The surface profiles on the samples produced with FOD were measured and the results are provided in Fig. 4. The height of the bulges (H) on the reference sample was the highest and then it decreased with the FOD increase as shown in Fig. 4a. At the same time, the depth of the channels (D) increased initially, as expected [24], and picked at FOD of 1 mm (see Fig. 4b) with two maximums, both above and below the focal plane. The width of the channels increased when FOD was above the focal plane, while initially decreased when FOD had negative values up to 1 mm but only marginally before it started increasing again as depicted in Fig. 4c.

The standard deviations of D were higher, and this can be attributed to the bigger volume of molten material deposited along the channels' edges that even led to closures of the laser path (see Fig. 3a). The other reason for this big standard deviation are the limitations of the focus variation technology, in particular its capabilities to inspect high aspect ratio channels. At the same time, DOF of the laser used in this research was calculated with Eq. 1 and it was 1500 µm. Thus, theoretically acceptable patterning results should be expected within a range of 750 µm above and below the focal plane.

The deviations of the resulting profiles from the reference one were calculated using Eq. 3 and plotted in Fig. 4d. The maximum deviations of H, D and W values were 87%, 196% and 64%, respectively, D was the most affected profile parameter by the FOD increase and therefore it could be considered a critical constrain in producing surfaces with designed topographies. Especially, the maximum deviations of D resulted from FOD values of 1000 μm and 750 μm, below and above the focal position, respectively, that were only marginally outside the calculated DOF. In the case of H and W, the deviations obtained within the calculated DOF were smaller than the 30% and 15% respectively, as can be seen in Fig. 4e.

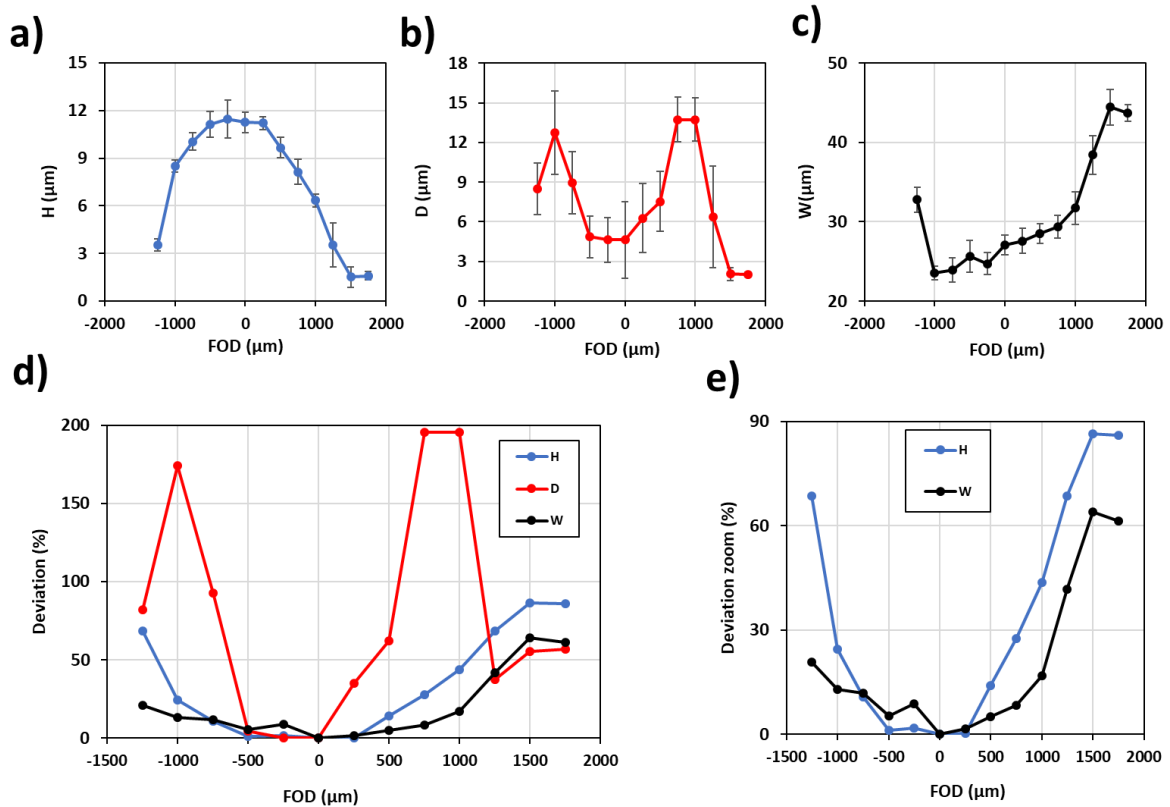**Fig. 4.** Surface profile parameters of samples produced with increasing FOD, i.e.: a) bulges' height, H; b) channels depth, D; c) channels width, W; and d-e) their deviations from the reference profile.

3.2.2. BIA effects

The evolution of surface profiles on the samples produced with BIA deviations from normal is depicted in Fig. 5. As it can be clearly seen, the bulges' height on both sides of the channels

was reduced almost equally, especially H_1 on beam incident side was only slightly higher than H_2 (see Fig. 5a). The channels depth, D, varied within a small range when BIA deviated from normal, however the standard deviation of the measurements was relatively high (see Fig. 5b) due to the same reasons as those in the case of FOD. The standard deviation of D was reduced with the BIA increase as the channels were getting wider (W increased as shown in Fig. 5c) and thus the measurement uncertainty was reduced. Furthermore, the W increase facilitated the evacuation of molten and vaporised material from the channels and this could explain the D increase when BIA was higher. At the same time, as expected the tapering angles, θ, increased progressively with the increase of BIA (see Fig. 5d) however this increase was much more pronounced on the beam incident side of the channels, i.e. for θ_1 that reached 64º when BIA was at 40º.

The deviations of the resulting profiles from the reference one were calculated using Eq. 3, again, and plotted in Fig. 5e. As expected, the deviations of all surface profile parameters increased with the increase of BIA.

As it was already stated the increase of θ_1 was significant and it was not surprising that the θ_1 deviation was the biggest, i.e. 150%, while the divisions for the other surface profile parameters were less than 50% for any BIA up to 35º (see Fig. 5e). Magnified views of θ, D and H & W deviations are provided in Fig. 5f-h, respectively. As it was already stressed, the BIA increase had a big impact on θ_1 and therefore, this profile parameter would be critical for obtaining surface profiles with acceptable deviations. In particular, θ_1 deviations were initially smaller for BIA up to 5º but then there was a steep increase to values higher than 30% at BIA of 10º (see Fig. 5f). At the same time the θ_2, deviations increased progressively to reach maximum values of approximately 30%. Regarding D, there was no clear trend that can be explained with the high standard deviations discussed before (see Fig. 5g) and the values did not exceed 50%. The trends for the other profile parameters, i.e. H and W, were very similar and the deviations were less than 15% for BIA up to 10º, and then they increased progressively (see Fig. 5h).
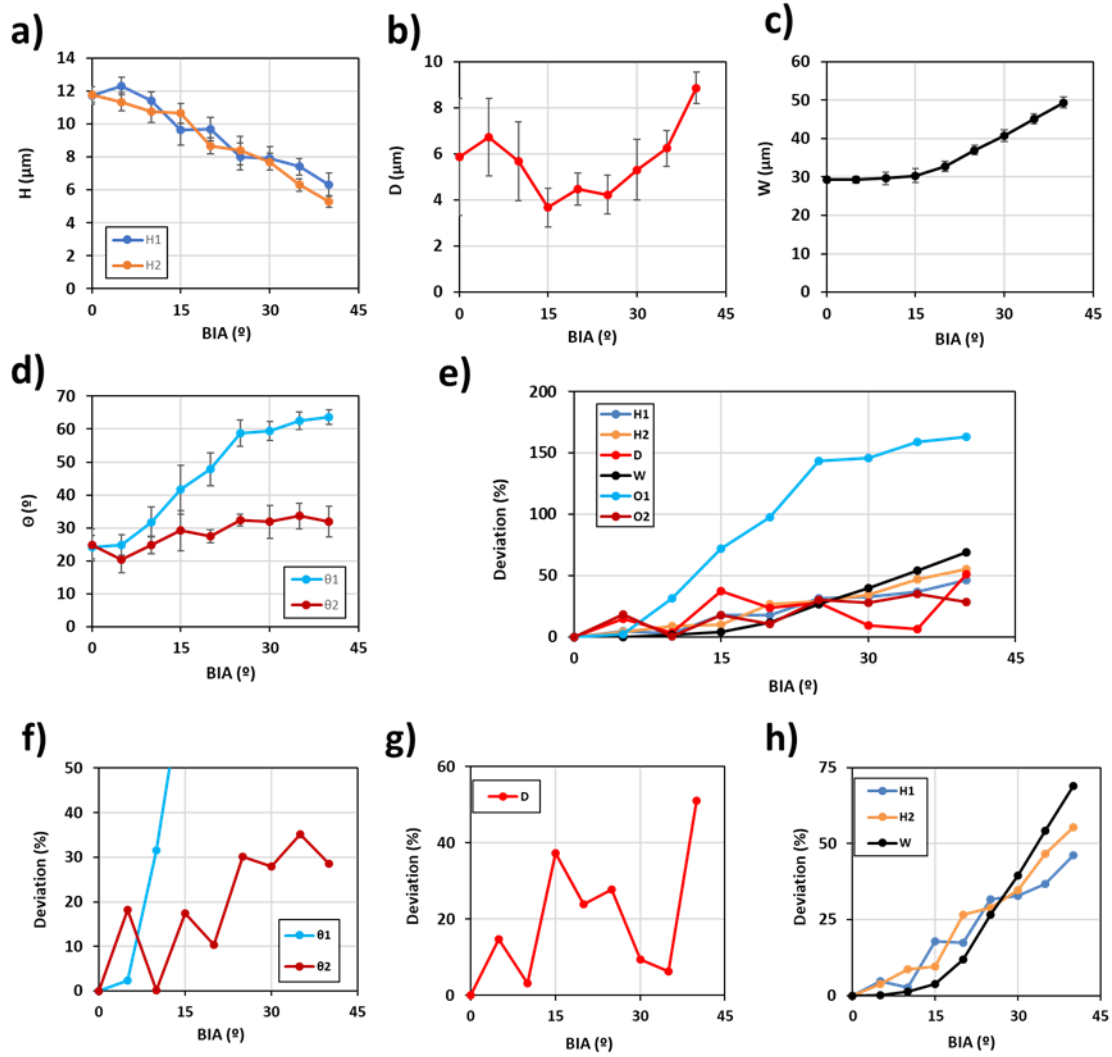
Fig. 5. Surface profile parameters of samples produced with varying BIA, i.e.: a) bulges' heights (H); b) channels' depth (D); c) channels' width (W), d) walls tapering angles (θ); and e-h) their deviations from the reference profile.

3.3. Effects on areal surface parameters

The effects of increasing FOD, BIA and the channel distance on areal surface parameters were analysed, i.e. Sa and Ar, were studied (see Section 2.2).

Fig. 6a-c plot Ar values obtained for the three sets of samples produced with the increasing channel distance, FOD and BIA. It was found that the Ar values peaked on the reference pattern (Ar = 1.57) and then decreased progressively with the increase of processing disturbances. As expected, the area factor decreased linearly with the increase of the channel distance as shown in Fig. 6a. The shift in the trend for the last two points could be explained with the bigger

distance between the channels and therefore there was less channels within the microscope field of view. The evolution of Ar with the FOD increase is depicted in Fig. 6b. Due to the higher ablation efficiency, i.e. higher D, and the reduced material deposition, i.e. lower H, when processing out of focus, the Ar values peak in focus. Then, there is a relatively small Ar decrease with the FOD increase up to 1mm while any further increases resulted in much steeper Ar decrease (see Fig. 6b). The BIA increase led to a progressive Ar decrease in line with the surface profile evolution, especially the increase of profile deviations (see Fig. 6c).

Sa is plotted in Fig. 6d-f, and again the Sa values peaked on the reference sample, i.e. Sa was 5.16 μm, and then decreased for the three sets of samples progressively with the increase of all three processing disturbances.
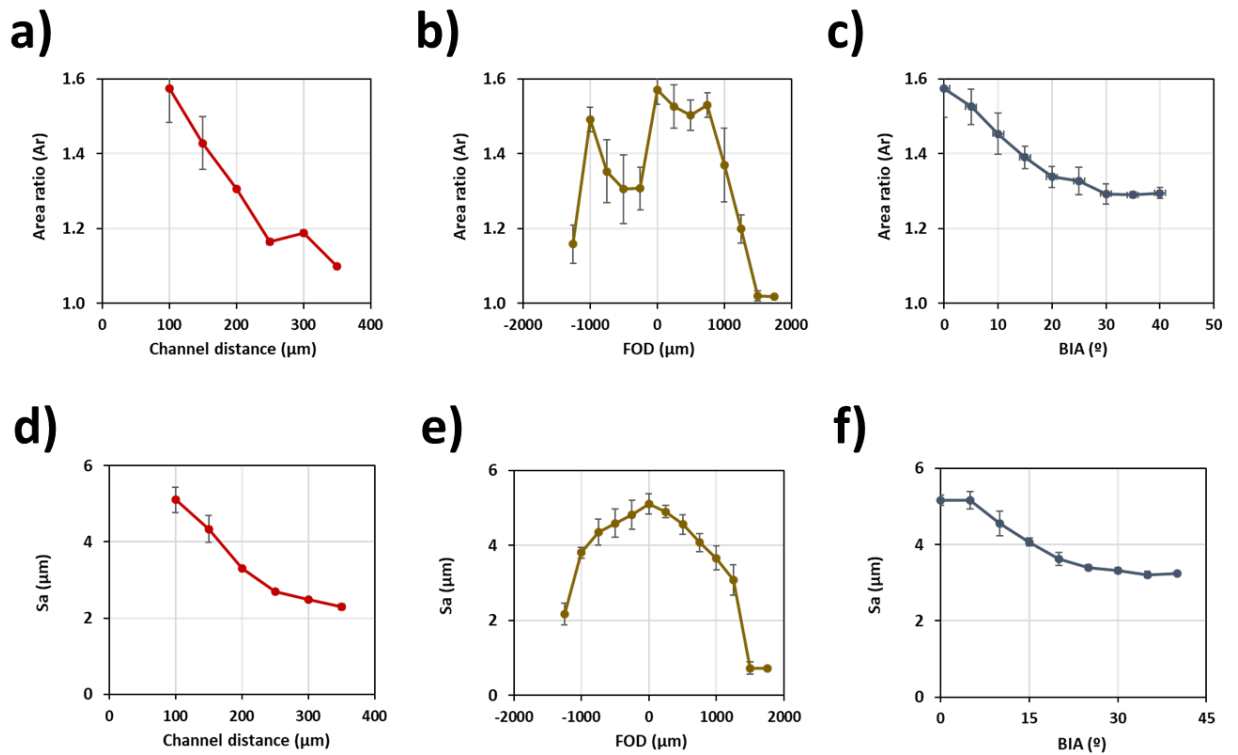

Fig. 6. Areal surface parameters: a-c) area ratios, Ar; and d-f) arithmetical mean heights, Sa, for the set of samples produced with the three processing disturbances, i.e. channel distance, FOD and BIA, respectively.

3.4. Effects on functional response

The relation between the functional response, i.e. the static contact angles (CA), of surfaces produced with increasing channel distance, FOD and BIA are depicted in Fig. 7a-c, respectively. The surfaces with a channel distance less than 200 μm were super hydrophobic, i.e. CA higher than 150º, as shown in Fig. 7a and then decreased progressively due to the decreasing roughness, indicated by both Sa and Ar in Fig. 6a and 6d. This surface functional response can be explained with the Cassie-Baxter state where as a result of the progressive roughness decrease there is less air trapped in the channels, especially the lower roughness leads to changes in the area fraction of the water-solid area to the projected area between the drops and the surface [34]. Furthermore, as the distance between channels increases, water drops can touch the untreated surface and spread and thus to reduce its hydrophobicity. There was a similar surface response to the FOD increase, especially the patterned surface remained super hydrophobic when FOD was less that 1mm, both above or below the focal plane, and then decreased progressively (see Fig. 7b). Again, this can be explained with the Cassie-Baxter state where due to the decreasing surface roughness (see Fig. 6b and 6e), there is less air trapped in the channels and also there is less absorption of airborne organic substances because of the smaller bulges and lesser porosity (see Fig. 3d) [15]. Regarding the other processing disturbance, super hydrophobicity of the patterned surface was not affected by the BIA increase and remained constant and higher than 160º (see Fig. 7c) in spite of the roughness decrease. This can be explained with the high surface porosity of the bulges (See Fig. 3e-f), and also the slower decrease of areal surface parameters i.e. both Sa and Ar (See Fig. 6c and 6f), and much lesser deviations of surface profile parameters compared with those resulting from the FOD increase. As the contact between drops and surfaces takes place onto the bulges, and the distance between the channels was maintained the same when BIA was varied, the drop-air surface did not change sufficiently to induce CA changes. Furthermore, as the BIA experiments were conducted at focus, i.e. with zero FOD, the porosity of the bulges was kept the same, and thus any CA changes in time should be attributed to the absorption of airborne organics. It is worth noting that the maximum BIA studied in this research was 40º, due to limitations in the laser processing setup, while the maximum tapering angle was approximately 60º. It could be expected that the tapering angles could increase to almost 90º if higher BIA than 40º were used and thus the contact between drops and surfaces would increase, too, in a decrement of air trapping, and hence could lead to a CA decrease.
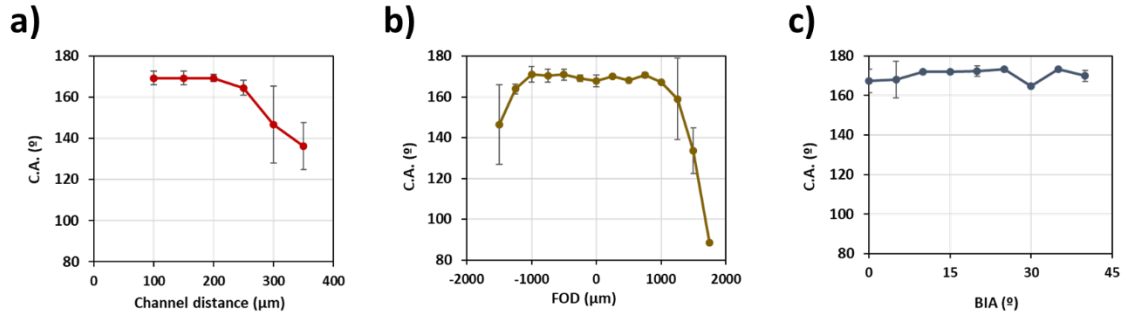
Fig. 7. Contact angles, CA, for the set of samples produced with the three processing disturbances, i.e. a) channel distance, b) FOD and c) BIA, respectively.

3.5. Correlations between disturbances, areal parameters and functional response

The resulting surface patterns were very sensitive to processing disturbances, i.e. FOD and BIA, that are commonly present in laser patterning of 3-D surfaces (see Section 3.2). However, it is even more important to determine how the evolution of resulting patterns as a result of increasing FOD, BIA and the channel distance affects the functional response of surfaces and if there is any correlation to the areal surface parameters. This is important as a potential solution for monitoring the laser patterning process and thus to use such correlations for triggering routines that can keep the process in control. Therefore, Pearson correlation analysis was conducted to examine the relationship between the functional response, i.e. the surface hydrophobicity, and either processing disturbances or the two areal surface parameters, i.e. Sa and Ar, investigated in this research, but also the correlation between the disturbances and the areal surface parameters.

The results of Pearson correlation analysis between the studied disturbances and the areal surface parameters of patterned surfaces together with their respective P-values are provided in Table 1. They confirm that the two parameters, i.e. Sa and Ar, considered in this research can be used to monitor whether the patterning process is in control. In particular, all Pearson correlation coefficients between disturbances and areal parameters are higher than 0.8, and very close to 1 in most of the cases, while the P-values are less than 0.05. Thus, there is a very strong correlation and Ar and Sa can be considered good indicators about the process performance. Especially, the process can be considered in control in regards to the resulting surface profiles,

and thus they can be employed for inline monitoring, e.g. by integrating a focus variation sensor in laser processing setups [35].

Regarding the functional response, there is a strong correlation with two disturbances, i.e. channel distance and FOD, but it is less pronounced compared with that to areal parameters and it is statically significant only in respect to FOD. At the same time, there is no correlation between BIAs and CAs as it has been already indicated in Fig. 7c.

The correlation between areal parameters and disturbances is very strong and thus by knowing the interrelation between the disturbances, i.e. channel' distance, FOD and BIA, and the functionality (see Fig. 7), it is possible indirectly to judge what will be the functional response. In particular, when 3-D surfaces are laser patterned and thus the three processing disturbances investigated in this research are present, the process can be considered as performing acceptably or the targeting hydrophobic properties are still present if Sa and Ar are higher than 3 µm and 1.3, respectively.

	FOD		Ch distance		BIA	
	Pearson	P-Value	Pearson	P-Value	Pearson	P-Value
Disturbance vs Sa	-0.93	0.0	-0.96	0.0024	-0.95	0.0001
Disturbance vs Ar	-0.80	0.0011	-0.96	0.0024	-0.94	0.0001
Disturbance vs CA	-0.70	0.0072	-0.89	0.0170	0.19	0.6285
Sa vs CA	0.82	0.0006	0.73	0.0973	-0.29	0.4427
Ar vs CA	0.73	0.0050	0.73	0.0979	-0.29	0.4546

Table 1. Pearson coefficients together with P-values for the investigated correlations between disturbances, areal parameters and contact angles.

3.6. Patterning of 3-D surfaces

The results obtained with the proposed methodology can be used to set constraints in pre-processing 3-D surfaces for follow up laser patterning and thus to maintain the desired functional response within acceptable limits while minimising the processing time. For example, the results from its pilot implementation in this research can be used to drive the partitioning/tessellation process when channel-like patterns are used for producing

hydrophobic surfaces, especially by setting limits on processing disturbances. In particular, the wettability achieved on the reference surfaces was maintained only when FOD was varying within the range from -1000 to 1000 μm and the distance between channels did not exceed 200 μm. At the same time BIA deviations had only a marginal effect and should be constrained to 60° as otherwise the channel distance can exceed 200 μm (see Section 3.4).

The proposed methodology for setting up constraints in pre-processing 3-D surfaces is generic and can be applied for producing different functional patterns and also on other materials than stainless steel. However, while the methodology is generic the produced topologies are dependent on the laser material interactions in any specific laser processing setup and also on the selected patterns for achieving a given functional response. Therefore, an empirical study as described in this research should be executed to determine what are the constrains on processing disturbances, i.e. pattern distortion, FOD and BIA deviations from normal, that should apply in pre-processing 3-D surfaces for any given functional pattern and workpiece material. And, again the functional response of three sets of samples should be investigated in order to set these constraints and thus to make sure that the desired functionality varies only within an acceptable range. All together, as it was already mentioned the results from such empirical studies can be used in proprietary software as Smartpatch and CALM to optimise the partitioning process.

4. Conclusions

A methodology is proposed in this research to investigate the effects of three process factors, also referred to as processing disturbances, i.e. pattern distortion, FOD and BIA, that can be present in laser patterning 3-D surfaces. A pilot implementation of this methodology is reported to illustrate how the effects of these processing disturbances on topographies, profiles and areal parameters together with the respective functional responses of patterned planar surfaces can be analysed and then used to set constraints in pre-processing 3-D surfaces for follow up laser patterning. The results are analysed in detail to show how such constraints can be set on channel-like patterns for producing surfaces with hydrophobic properties. In particular, the following conclusions can be made based on the results in this pilot implementation of the proposed methodology:

1. The analysis of the surface profile parameters has shown that the depth of the channels was the most sensitive to the FOD increase and therefore it is important process setting

up parameter in determining the laser patterning window. However, it is worth noting that DOF of a given laser source could be a good indicator for maintaining the surface profile parameters within acceptable limits because the depth maximum deviations were obtained when FOD exceeded DOF.

2. The BIA increase had a big impact on the tapering angle, especially on the beam incident side of the channels, and therefore this profile parameter could be critical when processing 3-D surfaces.

3. The areal surface parameters, i.e. Ar and Sa, can be considered good indicators about the process performance. A strong correlation between disturbances and these resulting surface parameters was demonstrated. Especially, they can indicate if the process is still performing acceptably in regards to the resulting surface profiles and thus can be used for inline monitoring of the laser patterning process.

4. Two processing disturbances, i.e. channel distance and FOD, had a similar effect on functional response of patterned surfaces, i.e. their hydrophobicity. In particular, the surfaces with a channel distance less than 200 μm were super hydrophobic and then hydrophobicity decreased progressively due to the increasing deviation from the reference patterns and decreasing roughness. There was a similar surface response to the FOD increase, especially the patterned surface remained super hydrophobic when FOD was less that 1mm, both above or below the focal plane, and then again decreased progressively.

5. The BIA increase did not have a negative effect on functional response of patterned surfaces, i.e. their hydrophobicity. In particular, super hydrophobicity of the patterned surface was not affected by the BIA increase in spite of the roughness decrease. This was attributed to the relatively slower decrease of the surface roughness and much lesser deviations of surface profile parameters except the bulges' height compared with those resulting from the FOD increase.

6. There was a strong correlation between two disturbances, i.e. channel distance and FOD, and the functional response of the laser patterned surfaces. At the same time, there was no correlation between BIAs and hydrophobicity and thus this confirmed that the surface functional response was not sensitive to the BIA increase. So, when patterning 3-D surfaces it would be necessary to introduce constraints regarding FOD and channel distance. In addition, due to the strong correlation between FOD/channel distance and areal surface parameters it will be possible by monitoring them to judge indirectly if hydrophobic properties are still present.

Acknowledgements

References

[1]   R. Liao, Z. Zuo, C. Guo, A. Zhuang, X. Zhao, Y. Yuan, Anti-icing performance in glaze ice of nanostructured film prepared by RF magnetron sputtering, Appl. Surf. Sci. 356 (2015) 539–545. doi:10.1016/j.apsusc.2015.08.103.

[2]   K. Glinel, P. Thebault, V. Humblot, C.M. Pradier, T. Jouenne, Antibacterial surfaces developed from bio-inspired approaches, Acta Biomater. 8 (2012) 1670–1684. doi:10.1016/j.actbio.2012.01.011.

[3]   A. Batal, R. Sammons, S. Dimov, Response of Saos-2 osteoblast-like cells to laser surface texturing, sandblasting and hydroxyapatite coating on CoCrMo alloy surfaces, Mater. Sci. Eng. C. 98 (2019) 1005–1013. doi:10.1016/j.msec.2019.01.067.

[4]   J.T. Cardoso, A. Garcia-Girón, J.M. Romano, D. Huerta-Murillo, R. Jagdheesh, M. Walker, S.S. Dimov, J.L. Ocaña, Influence of ambient conditions on the evolution of wettability properties of an IR-, ns-laser textured aluminium alloy, RSC Adv. 7 (2017) 39617–39627. doi:10.1039/C7RA07421B.

[5]   T. Stark, S. Alamri, A.I. Aguilar-Morales, T. Kiedrowski, A.F. Lasagni, Positive Effect of Laser Structured Surfaces on Tribological Performance, JLMN-Journal of Laser Micro/Nanoengineering. 14 (2019) 13–18. doi:10.2961/jlmn.2019.01.0003.

[6]   J. Bico, U. Thiele, D. Quéré, Wetting of textured surfaces, Colloids Surfaces A
        Physicochem. Eng. Asp. 206 (2002) 41–46. doi:10.1016/S0927-7757(02)00061-4.

[7]   X. Yao, Y. Song, L. Jiang, Applications of bio-inspired special wettable surfaces, Adv.
        Mater. 23 (2011) 719–734. doi:10.1002/adma.201002689.

[8]   Z. Wang, M. Elimelech, S. Lin, Environmental Applications of Interfacial Materials
        with Special Wettability, Environ. Sci. Technol. 50 (2016) 2132–2150.
        doi:10.1021/acs.est.5b04351.

[9]   P. Wang, T. Yao, B. Sun, T. Ci, X. Fan, H. Han, Fabrication of mechanically robust
        superhydrophobic steel surface with corrosion resistance property, RSC Adv. 7 (2017)
        39699–39703. doi:10.1039/c7ra06836k.

[10]   L. Mishchenko, B. Hatton, V. Bahadur, J.A. Taylor, T. Krupenkin, J. Aizenberg,
        Design of ice-free nanostructured surfaces based on repulsion of impacting water
        droplets, ACS Nano. 4 (2010) 7699–7707. doi:10.1021/nn102557p.

[11]   R. Jagdheesh, M. Diaz, J.L. Ocaña, Bio inspired self-cleaning ultrahydrophobic
        aluminium surface by laser processing, RSC Adv. 6 (2016) 72933–72941.
        doi:10.1039/C6RA12236A.

[12]   D. Bhaduri, P. Penchev, S. Dimov, S.L. Soo, An investigation of accuracy,
        repeatability and reproducibility of laser micromachining systems, Measurement. 88
        (2016) 248–261. doi:10.1016/J.MEASUREMENT.2016.03.033.

[13]   P. Penchev, S. Dimov, D. Bhaduri, S.L. Soo, Generic integration tools for
        reconfigurable laser micromachining systems, J. Manuf. Syst. 38 (2016) 27–45.
        doi:10.1016/j.jmsy.2015.10.006.

[14]   W.M. Steen, J. Mazumder, Laser Material Processing, Springer London, London,
        2010. doi:10.1007/978-1-84996-062-5.

[15]   D. Huerta-Murillo, A. García-Girón, J.M. Romano, J.T. Cardoso, F. Cordovilla, M.
        Walker, S.S. Dimov, J.L. Ocaña, Wettability modification of laser-fabricated
        hierarchical surface structures in Ti-6Al-4V titanium alloy, Appl. Surf. Sci. 463 (2019)
        838–846. doi:10.1016/j.apsusc.2018.09.012.

[16]   L.B. Boinovich, A.M. Emelyanenko, A.D. Modestov, A.G. Domantovsky, K.A.
        Emelyanenko, Synergistic Effect of Superhydrophobicity and Oxidized Layers on

Corrosion Resistance of Aluminum Alloy Surface Textured by Nanosecond Laser Treatment, ACS Appl. Mater. Interfaces. 7 (2015) 19500–19508. doi:10.1021/acsami.5b06217.

[17] S. Alamri, M. El-Khoury, A.I. Aguilar-Morales, S. Storm, T. Kunze, A.F. Lasagni, Fabrication of inclined non-symmetrical periodic micro-structures using Direct Laser Interference Patterning, Sci. Rep. 9 (2019) 5455. doi:10.1038/s41598-019-41902-x.

[18] J. Diaci, D. Bračun, A. Gorkič, J. Možina, Rapid and flexible laser marking and engraving of tilted and curved surfaces, Appl. Surf. Sci. 49 (2011) 195–199. doi:10.1016/j.optlaseng.2010.09.003.

[19] L. Overmeyer, J.F. Duesing, O. Suttmann, U. Stute, Laser patterning of thin film sensors on 3-D surfaces, CIRP Ann. - Manuf. Technol. 61 (2012) 215–218. doi:10.1016/j.cirp.2012.03.087.

[20] G. Cuccolini, L. Orazi, A. Fortunato, 5 Axes computer aided laser milling, Opt. Lasers Eng. 51 (2013) 749–760. doi:10.1016/j.optlaseng.2013.01.015.

[21] M. Jiang, X. Wang, S. Ke, F. Zhang, X. Zeng, Large scale layering laser surface texturing system based on high speed optical scanners and gantry machine tool, Robot. Comput. Integr. Manuf. 48 (2018) 113–120. doi:10.1016/j.rcim.2017.03.005.

[22] X. Wang, J. Duan, M. Jiang, S. Ke, B. Wu, X. Zeng, Study of laser precision ablating texture patterns on large-scale freeform surface, Int J Adv ManufTechnol. 92 (2017) 4571–4581. doi:10.1007/s00170-017-0413-z.

[23] P. Penchev, S. Dimov, D. Bhaduri, Experimental investigation of 3D scanheads for laser micro-processing, Opt. Laser Technol. J. 81 (2016) 55–59. doi:10.1016/j.optlastec.2016.01.035.

[24] D. Sola, A. Escartín, R. Cases, J.I. Peña, Laser ablation of advanced ceramics and glass-ceramic materials: Reference position dependence, Appl. Surf. Sci. 257 (2011) 5413–5419. doi:10.1016/J.APSUSC.2010.09.089.

[25] D. Sola, J. Peña, D. Sola, J.I. Peña, Study of the Wavelength Dependence in Laser Ablation of Advanced Ceramics and Glass-Ceramic Materials in the Nanosecond Range, Materials (Basel). 6 (2013) 5302–5313. doi:10.3390/ma6115302.

[26] D. V. Ta, A. Dunn, T.J. Wasley, R.W. Kay, J. Stringer, P.J. Smith, C. Connaughton,

J.D. Shephard, Nanosecond laser textured superhydrophobic metallic surfaces and their chemical sensing applications, Appl. Surf. Sci. 357 (2015) 248–254. doi:10.1016/j.apsusc.2015.09.027.

[27] Z. Zhang, Q. Gu, W. Jiang, H. Zhu, K. Xu, Y. Ren, C. Xu, Achieving of bionic super-hydrophobicity by electrodepositing nano-Ni-pyramids on the picosecond laser-ablated micro-Cu-cone surface, Surf. Coatings Technol. 363 (2019) 170–178. doi:10.1016/j.surfcoat.2019.02.037.

[28] A. Rodrigues, Technical article GF Machining Solutions ' latest -generation GF Laser Workstation Software revolutionizes Laser texturing by guaranteeing both quality and productivity, GF Mach. Solut. (2017).

[29] Fraunhofer IPT, CALM - Computer Aided Laser Manufacturing, Fraunhofer-Institut Für Produktionstechnologie IPT. (n.d.).

[30] K.M. Tanvir Ahmmed, A.-M. Kietzig, Drag reduction on laser-patterned hierarchical superhydrophobic surfaces, Soft Matter. 12 (2016) 4912–4922. doi:10.1039/c6sm00436a.

[31] S. Suzuki, A. Nakajima, K. Tanaka, M. Sakai, A. Hashimoto, N. Yoshida, Y. Kameshima, K. Okada, Sliding behavior of water droplets on line-patterned hydrophobic surfaces, Appl. Surf. Sci. 254 (2008) 1797–1805. doi:10.1016/j.apsusc.2007.07.171.

[32] A. Garcia-Giron, J.M. Romano, A. Batal, B. Dashtbozorg, H. Dong, E. Martinez Solanas, D. Urrutia, M. Walker, P. Penchev, S.S. Dimov, Durability and Wear Resistance of Laser-Textured Hardened Stainless Steel Surfaces with Hydrophobic Properties, Langmuir. 35 (2019) 5353–5363. doi:10.1021/acs.langmuir.9b00398.

[33] J.L. Ocaña, R. Jagdheesh, J.J. Garcia-Ballesteros, Direct generation of superhydrophobic microstructures in metals by UV laser sources in the nanosecond regime, Adv. Opt. Technol. 5 (2016) 87–93. doi:10.1515/aot-2016-0002.

[34] A. Garcia-Giron, J.M. Romano, Y. Liang, B. Dashtbozorg, H. Dong, P. Penchev, S.S. Dimov, Combined surface hardening and laser patterning approach for functionalising stainless steel surfaces, Appl. Surf. Sci. 439 (2018) 516–524. doi:10.1016/j.apsusc.2018.01.012.

[35]   V. Nasrollahi, P. Penchev, S. Dimov, L. Korner, R. Leach, K. Kim, Two-Side Laser
       Processing Method for Producing High Aspect Ratio Microholes, J. Micro Nano-
       Manufacturing. 5 (2017) 041006. doi:10.1115/1.4037645.